

First Annual Report on Development of Microwave Resonant Cavity Transducer for Fluid Flow Sensing

Development of Sensor Performance Model of Microwave Cavity Flow Meter for Advanced Reactor High Temperature Fluids

Nuclear Science and Engineering Division

About Argonne National Laboratory

Argonne is a U.S. Department of Energy laboratory managed by UChicago Argonne, LLC under contract DE-AC02-06CH11357. The Laboratory's main facility is outside Chicago, at 9700 South Cass Avenue, Argonne, Illinois 60439. For information about Argonne and its pioneering science and technology programs, see www.anl.gov.

Document availability

Online Access: U.S. Department of Energy (DOE) reports produced after 1991 and a growing number of pre-1991 documents are available free at OSTI.GOV (<http://www.osti.gov/>), a service of the U.S. Dept. of Energy's Office of Scientific and Technical Information

Reports not in digital format may be purchased by the public from the National Technical Information Service (NTIS):

U.S. Department of Commerce
National Technical Information Service
5301 Shawnee Rd
Alexandria, VA 22312
www.ntis.gov
Phone: (800) 553-NTIS (6847) or (703) 605-6000
Fax: (703) 605-6900
Email: orders@ntis.gov

Reports not in digital format are available to DOE and DOE contractors from the Office of Scientific and Technical Information (OSTI):

U.S. Department of Energy
Office of Scientific and Technical Information
P.O. Box 62
Oak Ridge, TN 37831-0062
www.osti.gov
Phone: (865) 576-8401
Fax: (865) 576-5728
Email: reports@osti.gov

Disclaimer

This report was prepared as an account of work sponsored by an agency of the United States Government. Neither the United States Government nor any agency thereof, nor UChicago Argonne, LLC, nor any of their employees or officers, makes any warranty, express or implied, or assumes any legal liability or responsibility for the accuracy, completeness, or usefulness of any information, apparatus, product, or process disclosed, or represents that its use would not infringe privately owned rights. Reference herein to any specific commercial product, process, or service by trade name, trademark, manufacturer, or otherwise, does not necessarily constitute or imply its endorsement, recommendation, or favoring by the United States Government or any agency thereof. The views and opinions of document authors expressed herein do not necessarily state or reflect those of the United States Government or any agency thereof, Argonne National Laboratory, or UChicago Argonne, LLC.

First Annual Report on Development of Microwave Resonant Cavity Transducer for Fluid Flow Sensing

Development of Sensor Performance Model of Microwave Cavity Flow Meter for Advanced Reactor High Temperature Fluids

prepared by

Alexander Heifetz¹, Sasan Bakhtiari¹, Eugene R. Koehl¹, Dmitry Shribak¹, David Aronson¹,
Tianyang Fang^{1,2}, Jafar Saniie²

¹Nuclear Science Engineering Division, Argonne National Laboratory

²Department of Electrical and Computer Engineering, Illinois Institute of Technology

September 30, 2021

Table of Contents

Table of Contents	1
List of Figures	2
Abstract	4
1. Introduction	5
2. Sensor Model	7
2.1. Analytical model of microwave resonant frequency shift	7
2.2. Computer simulations of microwave resonant frequency shift	9
3. Analysis of Sensor Mechanical Resilience	13
3.1. Analytical model	13
3.2. COMSOL numerical model	15
4. Fabrication of Sensor Prototype	18
4.1. Fabrication of microwave cavity	18
4.2. Fabrication of piping Tee adapter	20
4.3. Electronic measurement system	22
5. Preliminary Proof-of-Principle Tests	24
5.1. Setup for proof-of-principle dry test	24
5.2. Proof-of-principle dry test measurements	25
6. Conclusions	28
References	29

List of Figures

Figure 1 – (a) Conceptual drawing of waveguide-coupled microwave cylindrical cavity with flexible membrane. (b) Deflection of membrane due to dynamic fluid pressure changes cavity volume, which shifts microwave resonant frequency.....	5
Figure 2 – Visualization of TM_{011} mode in cylindrical cavity with $R=0.35$ in occurring at 15.4GHz. Flexible membrane with $d=10$ mil is at the top of the cylinder	9
Figure 3 – (a) Conceptual Figure 3. Frequency shift of TM_{011} mode resonant frequency of $R=0.35$ in and $d=10$ mil stainless steel cylinder due to liquid sodium flow-induced membrane deflections at 500°C. Frequency shifts are calculated with COMSOL RF module using curved membrane model Equation (2), with COMSOL RF using flat membrane model with equivalent amplitude $w_{avg} = w_0/3$, and analytically using Equation (10).	10
Figure 4 – Visualization of TE_{011} mode in right cylindrical cavity with $R=0.35$ in occurring at $f_0 = 22.2$ GHz. Flexible membrane with $d=10$ mil is at the top of the cylinder	11
Figure 5 – Frequency shift of TE_{011} mode resonant frequency shift of $R=0.4$ in and $d=10$ mil stainless steel cylinder due to liquid sodium flow-induced membrane deflections at 500°C. Frequency shift is calculated with COMSOL RF module using curved membrane model.....	11
Figure 6 – Visualization of TE_{012} mode in right cylindrical cavity with $R=0.35$ in occurring at $f_0 = 26.5$ GHz. Flexible membrane with $d=10$ mil is at the top of the cylinder	12
Figure 7 – Frequency shift of TE_{012} mode resonant frequency shift of $R=0.4$ in and $d=10$ mil stainless steel cylinder due to liquid sodium flow-induced membrane deflections at 500°C. Frequency shift is calculated with COMSOL RF module using curved membrane model.....	12
Figure 8 – Model of a thin circular plate	14
Figure 9 – Plot of σ_{max} as a function of h for (a) $v = 1$ m/s, (b) $v = 0.5$ m/s	15
Figure 10 – COMSOL calculation of Von Mises stresses for (a) $v = 1$ m/s, $h = 10$ mil, (b) $v = 0.5$ m/s, $h = 10$ mil, (c) $v = 0.5$ m/s, $h = 5$ mil.	17
Figure 11 – Side view and 3D visualization of the cylindrical cavity design.....	18
Figure 12 – Top view of the cavity and 3D visualization of waveguide coupling cavity side wall	19
Figure 13 – Brass K-band cylindrical cavity fabricated for proof-of-principle studies.....	19
Figure 14 – Brass cavity coupled to WR-42 bulkhead waveguide	20
Figure 15 – Leak-proof assembly consisting of a piping Tee and WR-42 bulkhead waveguide for insertion of microwave cavity into fluid stream	21
Figure 16 – Schematic drawing of adaptor for mounting WR-42 bulkhead waveguide in a piping Tee.....	21
Figure 17 – Photograph of adaptor and WR-42 bulkhead waveguide installed in piping Tee	22
Figure 18 – (a) Electronics and mechanics of the experimental setup for proof-of-principle testing (b) Waveguide microwave circulator is used for excitation and readout of microwave cavity ...	23
Figure 19 – Experimental setup for transducer dry test with a set of calibrated weights	24
Figure 20 – Dry test measurement of transducer response to pressure from a 50g weight	25

Figure 21 – GUI visualizing transducer response near 18.8GHz resonant frequency due to pressure applied calibrated weights: (a) 50g, (b) 100g.	26
Figure 22 – Transducer resonant frequency vs. applied pressure from 50g, 100g, 200g, and 500g weights. Responses are near cavity resonant frequencies (a) 18.8GHz, (b) 22.5GHz	27

Abstract

We are investigating a microwave cavity-based transducer for in-core high-temperature fluid flow sensing in molten salt cooled reactors (MSCR) and sodium fast reactors (SFR). This sensor is a hollow metallic cylindrical cavity, which can be fabricated from stainless steel, and as such is expected to be resilient to radiation, high temperature and corrosive environment of MSCR and SFR. The principle of sensing consists of making one wall of the cylindrical cavity flexible enough so that dynamic pressure, which is proportional to fluid velocity, will cause membrane deflection. Membrane deflection causes cavity volume change, which leads to a shift in the resonant frequency. Feasibility of the sensor was initially investigated with analytical derivations and with COMSOL RF Module computer simulations of resonant frequency spectral shift due to uniform load. We also investigated the mechanical integrity of the flowmeter's membrane through analytical modelling and COMSOL Structural Mechanics Module computer simulations. Both the analytic model and COMSOL model showed that maximum stresses on the plate, which are at the radial boundary of the plate, are three orders of magnitude smaller than the material's yield strength and ultimate tensile strength. This indicates that the sensor is at a low risk of mechanical failure. Using results from models, we have developed an initial design for a microwave K-band sensor. A cylindrical resonator prototype was fabricated from brass for the initial tests. The external dimensions of the cavity are matched to the flange of a standard WR-42 waveguide. Microwave field is coupled into the resonant cavity through a subwavelength-size aperture. A test article was developed consisting of a piping Tee with a bulkhead WR-42 microwave waveguide installed in a leak-proof assembly. A microwave waveguide circulator was installed in the setup to suppress the effect of reflections at the cavity entrance by increasing the isolation between the input and the output port. Preliminary spectral characterization of cavity spectral response was performed with a portable PXIe chassis microwave VNA with a custom GUI. Preliminary dry tests of the transducer response were conducted with a set of calibrated weights. Transducer frequency shift was shown to be monotonically increasing with increasing pressure. The next steps will involve investigation of the transducer performance for water flow sensing.

1. Introduction

High-temperature fluid reactors, such as sodium fast reactors (SFR) and molten salt cooled reactors (MSCR) are a promising advanced reactor option with highly efficient thermal energy conversion cycle [1,2]. Measurement of high-temperature fluid process variables, in particular the flow inside the pressure vessel, is a challenging task because of the harsh environments of advanced reactors, which includes radiation, high temperature, and contact with highly corrosive coolant fluid [3,4]. Molten salt flow sensors are typically ultrasonic ones [5]. Ultrasonic transducers are typically placed outside the vessel and pipes, but sensing requires a direct line-of-sight between the transducers. We are investigating a microwave cavity-based transducer for high-temperature fluid flow measurement for in-core sensing [6,7]. This sensor is a hollow metallic cavity, which can be fabricated from stainless steel, and as such is expected to be resilient to radiation, high temperature and corrosive environment of SFR and MSCR. A schematic drawing of the flow sensor is shown in Figure 1. The principle of sensing consists of making one wall of the cylindrical resonant cavity flexible enough so that dynamic pressure, which is proportional to fluid velocity, will cause membrane deflection. A cavity is characterized by its resonant frequencies, which occur due to constructive interferences of microwave field inside the cavity. Membrane deflection causes a change in cavity volume, and thus a shift in the resonant frequency. Using signal readout from microwave frequency shift in a hollow cavity is advantageous for applications in high temperature and high radiation environment, because no electronic components are placed inside the transducer. Energy coupling to and from the sensor will be achieved through a microwave waveguide, which will be an integral part of the insertion probe. A waveguide is a rigid narrow hollow metallic tube which is also resilient to high temperature and high-radiation environment. In the drawing in Figure 1, microwave field is coupled into the cylindrical resonant cavity through a side wall.

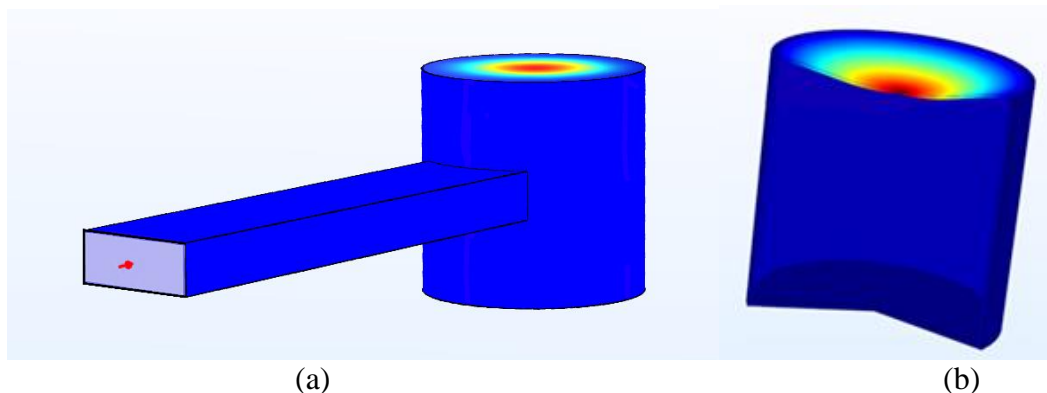


Figure 1 – (a) Conceptual drawing of waveguide-coupled microwave cylindrical cavity with flexible membrane. (b) Deflection of membrane due to dynamic fluid pressure changes cavity volume, which shifts microwave resonant frequency.

The work described in this report consists of transducer prototype design, fabrication, and proof-of-principle demonstration. Initial investigation of the transducer design parameters was

performed through analytic derivations and computer simulations using the COMSOL software package. This includes a study of signal sensitivity to displacement of the membrane due to dynamic fluid pressure, and the dependence of sensitivity on transducer geometrical parameters.

We also investigated the mechanical integrity of the flowmeter's membrane through computer simulations. By calculating the stress on the plate due to deflection and, comparing the stress to the material ultimate tensile strength and yield strength, it can be estimated if the plate will fail under representative test conditions. The stress on the plate was calculated with an analytic closed form solution model, and with COMSOL Structural Mechanics Module which does not involve any approximations. Both the analytic model and the COMSOL model showed that maximum stresses on the plate, which are at the radial boundary of the plate, are three orders of magnitude smaller than the material's yield strength and ultimate tensile strength. This indicates that the sensor is at a low risk of mechanical failure.

Computer analysis was followed by fabricating a K-band microwave cavity prototype for proof-of-principle flowmeter tests in water. Cylindrical cavity with the size matching the dimensions of a standard WR-42 waveguide flange was fabricated from brass for the initial performance characterizations. The cavity was coupled to a bulkhead WR-42 waveguide, which was connected to a waveguide microwave circulator. The circulator was installed in the setup to suppress the effect of reflections at the cavity entrance by increasing the isolation between the input and the output port. A test article with a leak-proof insert connecting the microwave sensor to a piping Tee was developed. A portable PXIe chassis microwave vector network analyzer was incorporated into the test setup. The PXIe graphical user interface (GUI) software has background subtraction and signal averaging capabilities for processing and display of the data.

Preliminary spectral characterization of the cavity response was performed under dry test conditions using a set of calibrated weights. Application of the mechanical pressure to the cavity membrane showed a clearly measurable shift in the resonant frequency. When pressure was released, cavity spectrum returned to the original state, indicating that measurements are repeatable. Good response at several resonant frequencies was observed, indicating the possibility of performing frequency sweep and coincidence detection to increase the fidelity of measurements.

2. Sensor Model

2.1. Analytical model of microwave resonant frequency shift

The model of the sensor combines elements of fluid and solid mechanics, and electrodynamics. Dynamic pressure q due to incompressible fluid flow normal to the membrane is given by Bernoulli equation:

$$q = \frac{1}{2} \rho v^2 \quad (1)$$

Where ρ and v are the fluid density and the flow velocity, respectively. For uniform pressure, deflection of circular membrane of radius R as a function of radial position r can be calculated using Timoshenko's model for radially constrained circular plate [7,8]

$$w(r) = \frac{PR^4}{64D} \left(1 - \frac{r^2}{R^2}\right)^2 = w_0 \left(1 - \frac{r^2}{R^2}\right)^2 \quad (2)$$

Where D is material flexural rigidity given as

$$D = \frac{Ed^3}{12(1-\nu^2)} \quad (3)$$

Here d is the plate thickness, E and ν are the plate material Young's modulus and Poisson ratio, respectively. Maximum plate deflection occurs at the center and can be expressed as

$$w(0) = w_0 = \frac{PR^4}{64D} = \rho v^2 \frac{3(1-\nu^2)}{32E} \frac{R^4}{d^3} \quad (4)$$

and the average plate deflection is given as

$$w_{avg} = \frac{1}{\pi R^2} \int_0^{2\pi} \int_0^R w(r) r dr d\phi = \frac{w_0}{3} \quad (5)$$

Resonant frequencies of transverse electric TE_{nml} modes of a cylindrical cavity are characterized by integers n, m, l [7,8]

$$f_{nml}^{TE} = \frac{c}{2\pi\sqrt{\mu_r\epsilon_r}} \sqrt{\left(\frac{X'_{nm}}{R}\right)^2 + \left(\frac{l\pi}{L}\right)^2} \quad (6)$$

in which μ_r and ϵ_r are permeability and permittivity of the medium, respectively, and X'_{nm} is the n^{th} root of the derivative of the m^{th} order Bessel function. The TM modes are described by a similar equation, with the difference that X'_{nm} is replaced with X_{nm} , the n^{th} root of the m^{th} order Bessel function. For an air-filled cavity, $\mu_r=1$ and $\epsilon_r=1$. The quality factor Q of a cavity is defined as

$$Q = \frac{f_0}{\Delta f_{FWHM}} \quad (7)$$

where f_0 is the resonant frequency, and Δf_{FWHM} is the full width at half maximum of the spectral linewidth. The Q of a gas-filled cavity is related to resistive losses at the walls, which are determined by the material electrical conductivity. When optimizing Q with respect to cavity geometry, the maximum Q value for low order modes such as TE_{01p}, is achieved when $L=2R$. The cavity resonant frequency for TE modes can be characterized by a single parameter

$$f_{nmp}^{TE} = \frac{c}{2\pi L} \sqrt{(2X'_{nm})^2 + (l\pi)^2} = \frac{c}{2L} g^{TE}(n, m, l) \quad (8)$$

and similarly for TM mode frequencies, where $g^{TE}(n, m, l)$ and $g^{TM}(n, m, l)$ are non-dimensional function of the mode number integers n, m, l . Depending on the cavity material, the value of Q for a low order mode of the cylindrical cavity could be as high as 20,000.

For small changes in the cavity height due to membrane displacement of magnitude ΔL , frequency shift is given, to first order in ΔL , as

$$\Delta f = \frac{df}{dL} \Delta L = -\frac{c}{2L^2} \Delta L g(n, m, l) \quad (9)$$

For $\Delta L = -w_{avg} = -w_0/3$, and using $L=2R$,

$$\Delta f = g(n, m, l) \frac{1-\nu^2}{256E} \frac{cR^2}{d^3} \rho v^2 \quad (10)$$

With respect to geometrical parameters of the cavity, detection sensitivity increases quadratically with R , and inverse cubic with d . With respect to fluid parameters, detection sensitivity increases linearly with density and quadratically with velocity.

Properties of materials and fluid variables which enter into Equation (10) are functions of temperature. For stainless steel 316, Young's modulus E , shear modulus G , and Poisson ratio ν are given as [9]

$$E = 2.137 \times 10^5 - 102.74T \quad (11a)$$

$$G = 8.964 \times 10^4 - 53.78T \quad (11b)$$

$$\nu = E/2G - 1 \quad (11c)$$

Where E and G are given in MPa, T is given in °C, and the correlations are valid for $0 < T < 800^\circ\text{C}$.

Temperature-dependent values of liquid sodium density ρ in units of kg/m³ is given by the correlation [10]

$$\rho = \rho_c + f(1-T/T_c) + g(1-T/T_c)^h \quad (12)$$

is valid for $371\text{K} < T < 2503.7\text{K}$, where $\rho_c=219$, $f=275.32$, $g=511.58$, $h=0.5$, $T_c=2503.7\text{K}$.

For molten salt, density decreases linearly with temperature. For example, for FLiBe (LiF-BeF₂), density correlation in units of kg/m³ is given by [11]

$$\rho = 2415.6 - 0.49072T \quad (13)$$

where T is in units of K. The correlation is valid for $732.2\text{K} < T < 4498.8\text{K}$.

2.2. Computer simulations of microwave resonant frequency shift

To confirm the validity of the analytical model approximations, resonant frequency shift of a microwave cavity was calculated with COMSOL RF module. The modes of cylindrical cavity in order of increasing frequency are TM_{010} , TM_{011} , TM_{012} , TE_{011} , TE_{012} , etc. The lowest frequency mode TM_{010} exhibits no variation of the E-field with length, and therefore it is almost insensitive to length change. The subsequent modes, however, are sensitive to change in cavity volume resulting from membrane displacement. A cavity with $R = 0.35\text{in}$, which matches the size of the cavity developed and characterized in prior work for a different application [12], was used in the initial study. The COMSOL simulation results for a $R=0.35\text{ in}$ and $d=10\text{ mil}$ membrane cylindrical cavity in Figure 2 shows the spatial distribution of the electric field in the cavity for TM_{011} mode, occurring at 15.4GHz . The flexible membrane is at the top of the cylinder.

Using stainless-steel and liquid sodium material property values at 500°C given by Equations (11) and (12), respectively, we estimate Δf for a range of velocity values from 0.5 m/s to 2 m/s . Frequency shifts were calculated with COMSOL RF module for TM_{011} mode. COMSOL simulations were performed for a parabolic membrane deflection profile given by Equation (2), and for a flat membrane displacement with amplitude $w_{\text{avg}} = w_0/3$ according to Equation (5). For comparison, frequency shift was also calculated using the analytical model of Equation (10). The results are plotted in Figure 3. Notice that the COMSOL RF calculations for parabolic membrane deflection shape and for equivalent amplitude flat membrane displacement agree closely, and also agree reasonably well with the frequency shifts calculated using the analytical model of Equation (10).

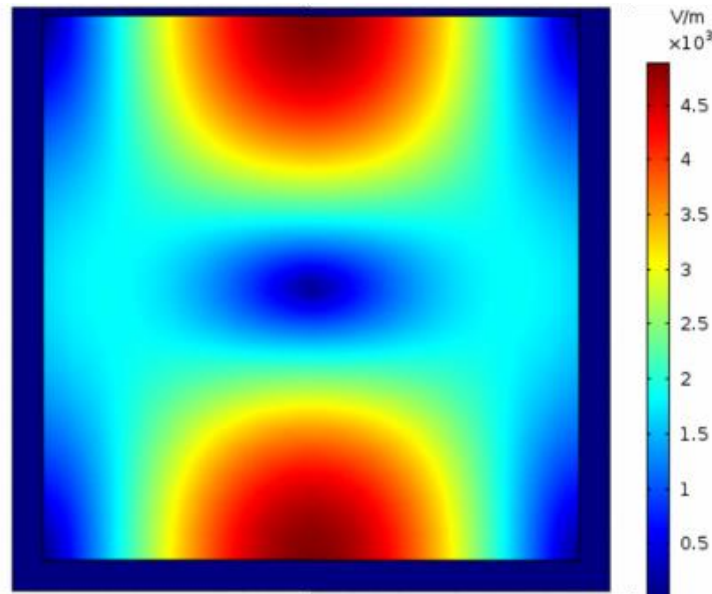


Figure 2 – Visualization of TM_{011} mode in cylindrical cavity with $R=0.35\text{ in}$ occurring at 15.4 GHz . Flexible membrane with $d=10\text{ mil}$ is at the top of the cylinder.

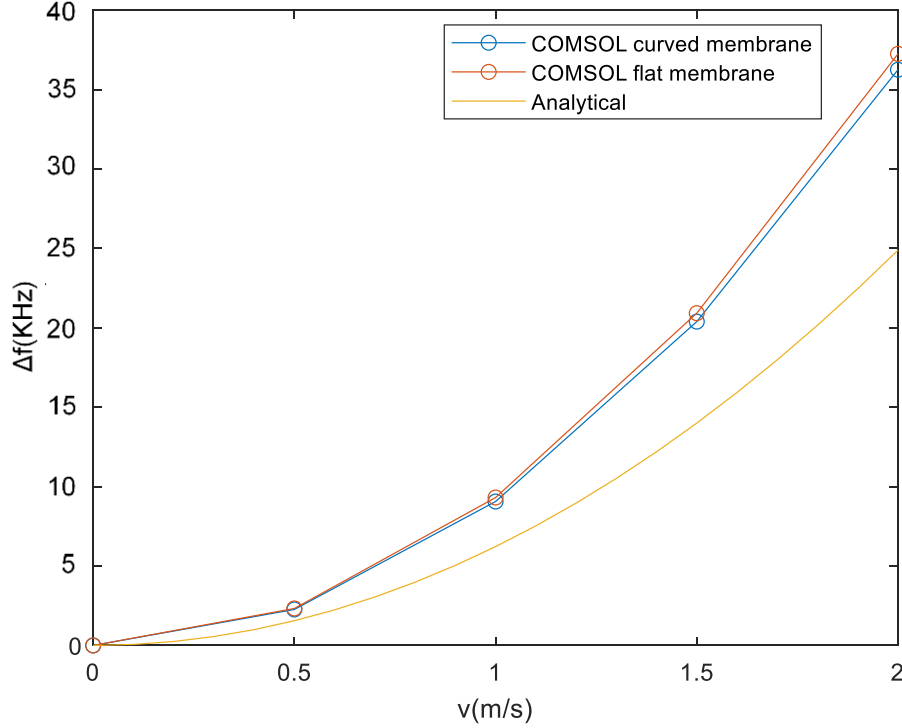


Figure 3 – (a) Frequency shift of TM_{011} mode resonant frequency of a stainless steel cylinder with $R=0.35$ in and $d=10$ mil due to liquid sodium flow-induced membrane deflections at 500°C . Frequency shifts are calculated with COMSOL RF module using curved membrane model of Equation (2), with COMSOL RF using flat membrane model with equivalent amplitude $w_{\text{avg}}=w_0/3$, and analytically using Equation (10).

Higher frequency modes, such as TE_{011} and TE_{012} modes, are known to have higher Q values than TM modes. Thus, we expect TE_{011} and TE_{012} modes to have better sensitivity to membrane displacement. Signal sensitivity for these two modes has been investigated through computer simulations, with results shown in Figures 4, 5, 6, and 7. COMSOL simulation results for $R=0.35$ in and $d=10$ mil right cylindrical cavity in Figure 4 show spatial distribution of the electric field in TE_{011} mode, occurring at 22.2 GHz resonant frequency with $Q = 17,900$. Resonant frequency shifts of the stainless steel cavity were calculated with COMSOL RF module for TE_{011} mode for a range of velocities (0.5 m/s to 2 m/s) of liquid sodium flow at 500°C . The membrane deflection profile was modeled using Equation (2). Results of computer simulations for the frequency shift are shown in Figure 5. As expected, for the same fluid velocity, frequency shifts of TE_{011} mode are larger than those of the TM_{011} mode.

COMSOL simulation results for a $R=0.35$ in and $d=10$ mil right cylindrical cavity in Figure 6 show spatial distribution of the electric field in TE_{012} mode occurring at 26.5 GHz resonant frequency with $Q = 19,500$. Frequency shifts for TE_{012} mode for a range of velocities (0.5 m/s to 2 m/s) of liquid sodium flow at 500°C are displayed in Figure 7. Because of the higher Q value and spatial distribution profile, frequency shifts for TE_{012} are higher than those of TE_{011} mode. As

discussed in Section 3.1, frequency shifts larger than 3 KHz are, in principle, detectable with modern electronic devices.

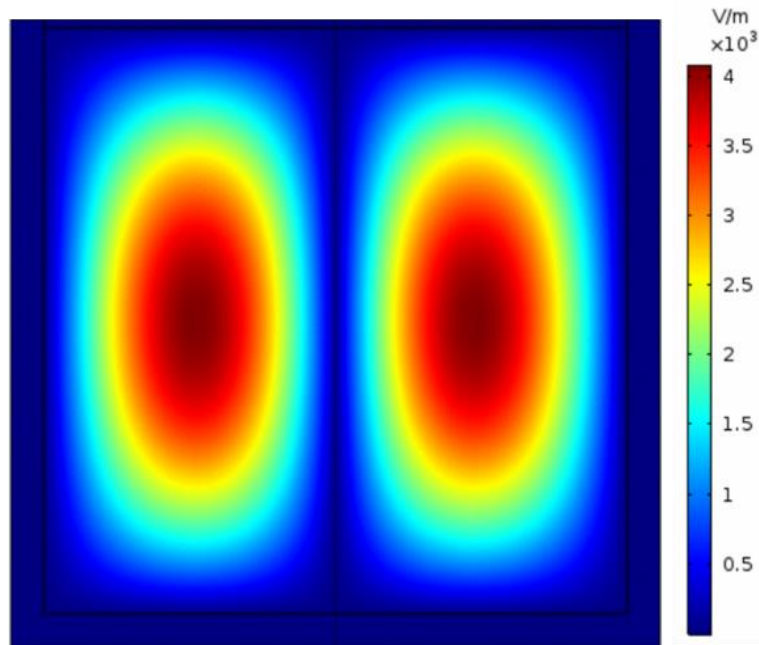


Figure 4 – Visualization of TE₀₁₁ mode in right cylindrical cavity with $R=0.35$ in occurring at $f_0 = 22.2$ GHz. Flexible membrane with $d=10$ mil is at the top of the cylinder

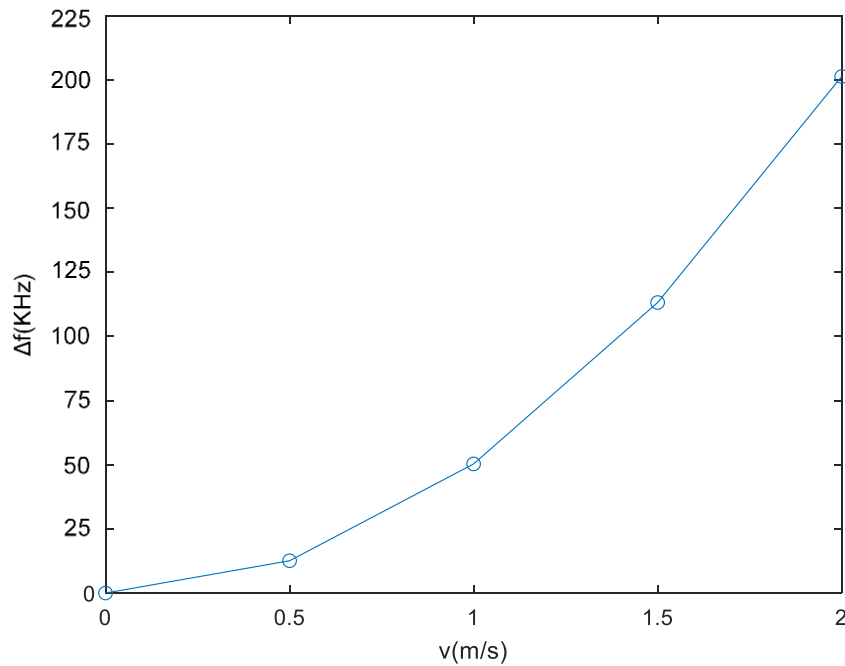


Figure 5 – Frequency shift of TE₀₁₁ mode resonant frequency of a $R=0.35$ in and $d=10$ mil stainless steel cylinder due to liquid sodium flow-induced membrane deflections at 500°C. Frequency shift is calculated with COMSOL RF module using the curved membrane model.

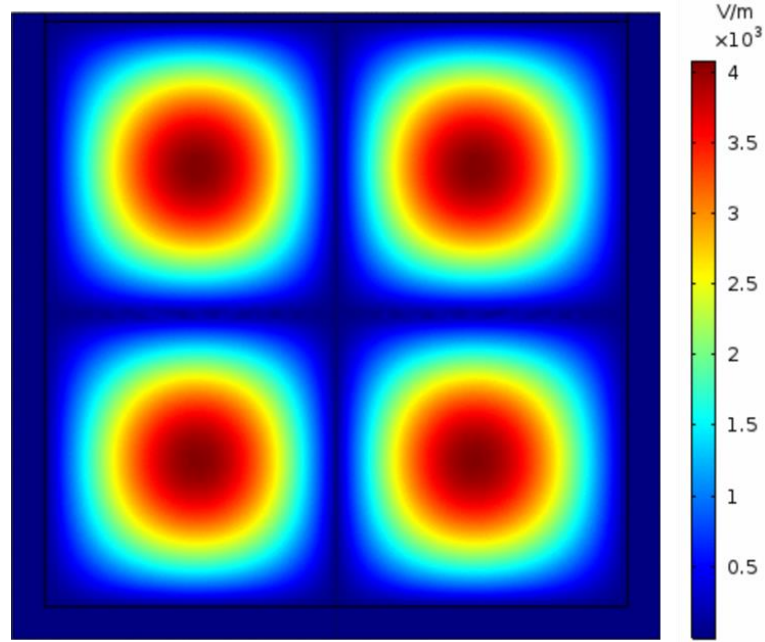


Figure 6 – Visualization of TE_{012} mode in a right cylindrical cavity with $R=0.35$ in occurring at $f_0 = 26.5\text{GHz}$. Flexible membrane with $d=10$ mil is at the top of the cylinder

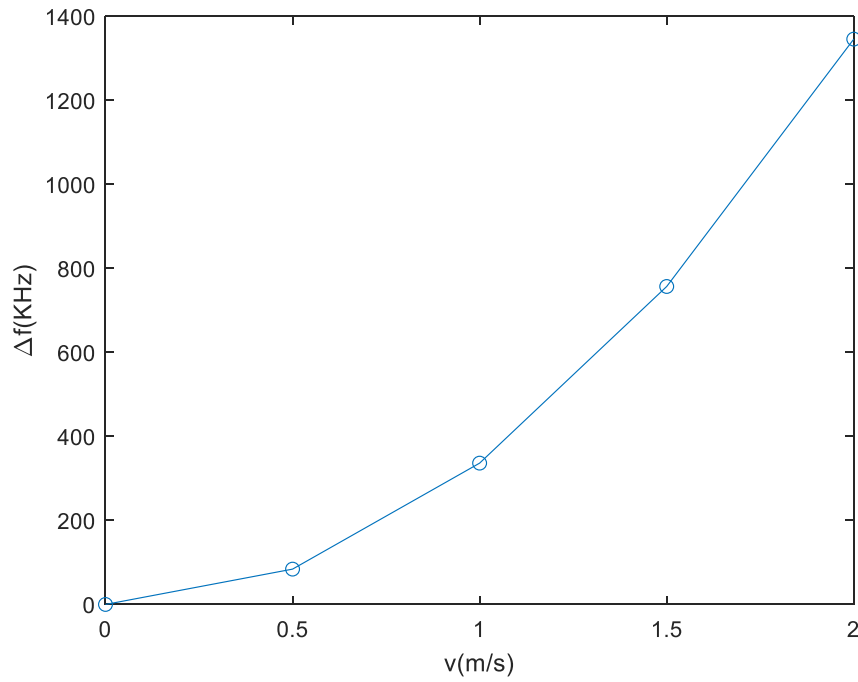


Figure 7 – Frequency shift of TE_{012} mode resonant frequency of $R=0.35$ in and $d=10$ mil stainless steel cylinder due to liquid sodium flow-induced membrane deflections at 500°C . Frequency shift is calculated with COMSOL RF module using the curved membrane model

3. Analysis of Sensor Mechanical Resilience

3.1. Analytical model

Thickness of the membrane is a critical parameter that affects sensor sensitivity. The value of thickness of the membrane is selected as a tradeoff between sensitivity and structural integrity of the sensor. One of the possible pathways to sensor failure is corrosion of the membrane. Prior studies indicate that stainless steel 316 is highly resistant to corrosion in liquid sodium. The available data is usually based on converting the weight change of thin samples to loss rates in mils per year, and thus might not account for local inter-granular penetration damage which could affect the mechanical properties. The data indicates that corrosion of stainless steel in liquid sodium depends on the concentration of oxide impurities, sodium flow velocity, and temperature. One study showed that, when the maximum temperature of the liquid sodium is 600°C, the oxide level is less than 10 ppm, and the velocity is 2 m/s, the corrosion rate at 2500 hours is approximately 2.3 $\mu\text{m}/\text{year}$ [13]. If the velocity is increased to 6 m/s, the corrosion rate is approximately 2.8 $\mu\text{m}/\text{year}$, indicating that the velocity has only a slight effect on the corrosion rate. However, if the velocity is held at 6m/s, and the maximum temperature is increased to 720°C, the corrosion rate is increased roughly by one order of magnitude to approximately 30.2 $\mu\text{m}/\text{year}$. In the case of molten salt, 2 $\mu\text{m}/\text{year}$ corrosion rate of SS316 was observed in purified FLiBe (2LiF-BeF₂) at 650°C in a static cell (no flow) [14,15]. However, another study of SS316 in FLiBe estimated the corrosion rate at 700°C to be between 17.1 $\mu\text{m}/\text{year}$ and 31.2 $\mu\text{m}/\text{year}$. In the liquid sodium environment of the Mechanisms Engineering Test Loop (METL) facility at Argonne [16], the operating conditions are maximum temperature of 650°C, liquid sodium velocity in pipes under 1 m/s, and oxide concentration of <5 ppm. The corrosion rate of SS316 is expected to be approximately 0.1 mil/year. Thus, in a 10-year life span, the sensor membrane, on average, could corrode by 1 mil. We choose $d=10$ mil (254 μm), so that corrosion would affect no more than 10% of the membrane. This number corresponds to a commonly available stainless steel stock sheet.

In analyzing mechanical integrity of the membrane of the transducer shown in Figure 1, it is sufficient to consider an isolated model of a uniformly loaded thin stainless-steel circular plate fixed at the radial boundary. An example of a thin circular plate is show in Figure 8. The objective is to determine if for the sensor membrane dimensions and flow rates identified in Section 2, maximum stresss on the membrane exceed YS and UTS values. For stainless steel 316, YS = 290 MPa and UTS = 580 MPa [17].

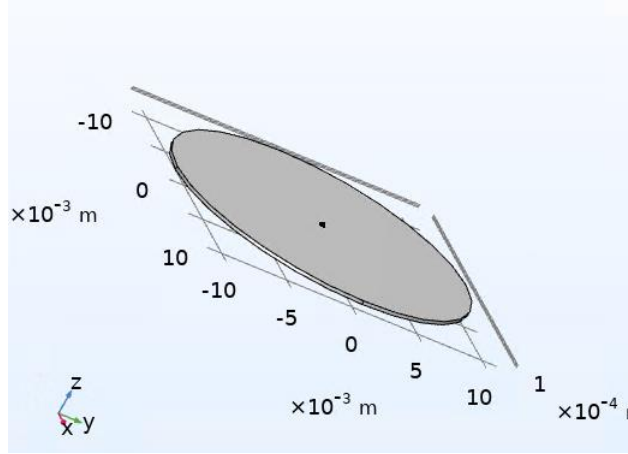


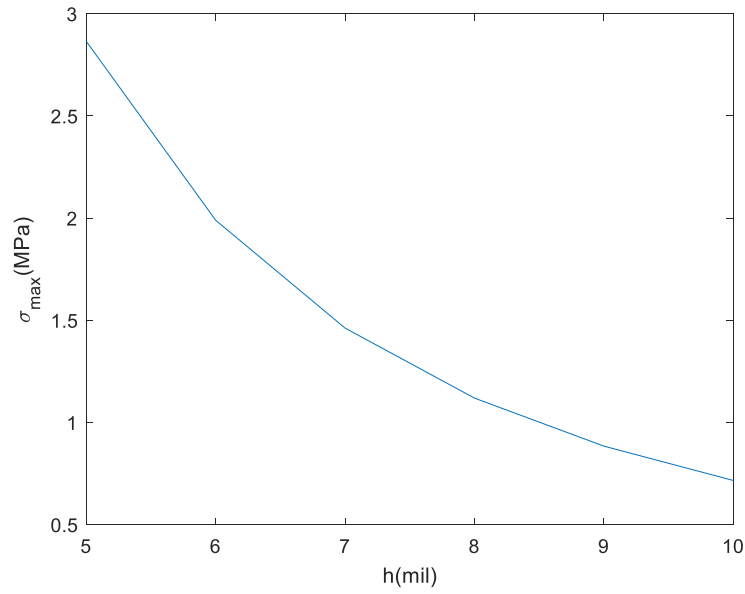
Figure 8 – Model of a thin circular plate

The plate in Figure 8 has radius a and thickness h . In the analysis of this report, radius is fixed with the value $a = 11.1$ mm. Thickness h is in the range of 5 mil to 10 mil. A closed form analytic solution for deflection of the plate has been developed in literature [8]. The maximum stress on the plate is at the radial boundary, and is given as

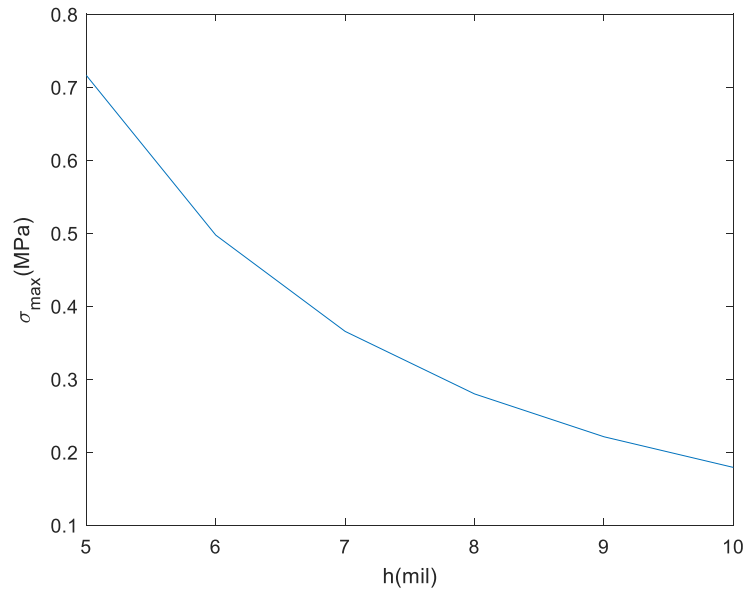
$$\sigma_{\max} = \frac{3}{4} q \frac{a^2}{h^2} \quad (14)$$

Where q is the pressure on the plate. Dynamic fluid pressure is related to fluid velocity and density according to Equation (1). The maximum stress is weakly dependent on temperature through temperature-dependent fluid density. For example, for FLiBe (LiF-BeF₂), density correlation in units of kg/m³ is given by Equation (13). Density changes by less than 1% for 100K change in temperature. Water density at 20°C is 1000 kg/m³, while density of liquid sodium at 530°C is 828 kg/m³ according to Equation (12), and density of FLiBe at 550°C is 2012 kg/m³ according to Equation (13). For order of magnitude calculations, differences in fluid densities by a factor of two can be neglected.

The graph in Figure 9 shows a plot of σ_{\max} as a function of h for representative velocity values of $v = 1$ m/s in Figure 9(a), and $v = 0.5$ m/s in Figure 9(b). The fluid is taken to be water at room temperature. The maximum stresses in Figures 9(a) and 9(b) are approximately 3 MPa and 0.7 MPa, respectively. These values are three orders of magnitude smaller than YS and UTS of stainless steel, which suggests that the risk of mechanical failure is low.



(a)



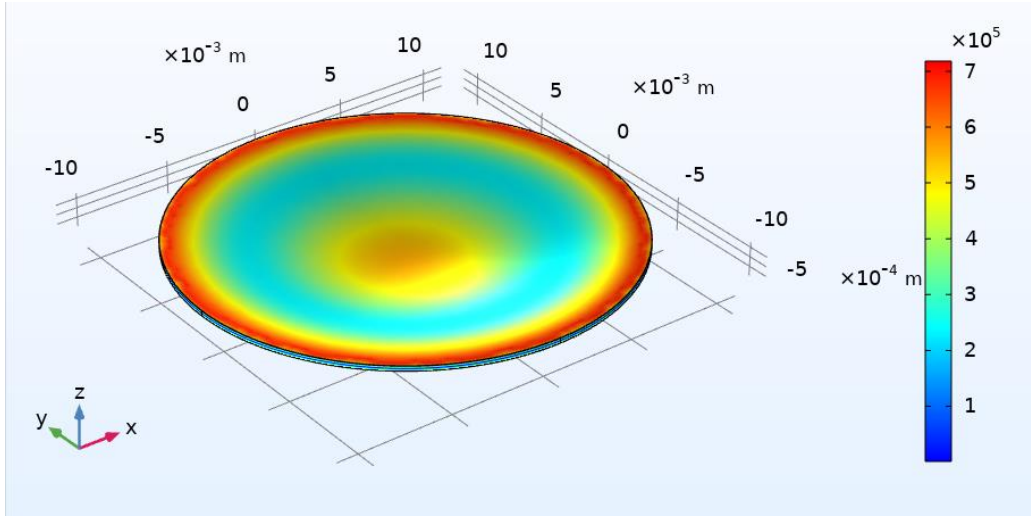
(b)

Figure 9 – Plot of σ_{\max} as a function of h for (a) $v = 1$ m/s, (b) $v = 0.5$ m/s

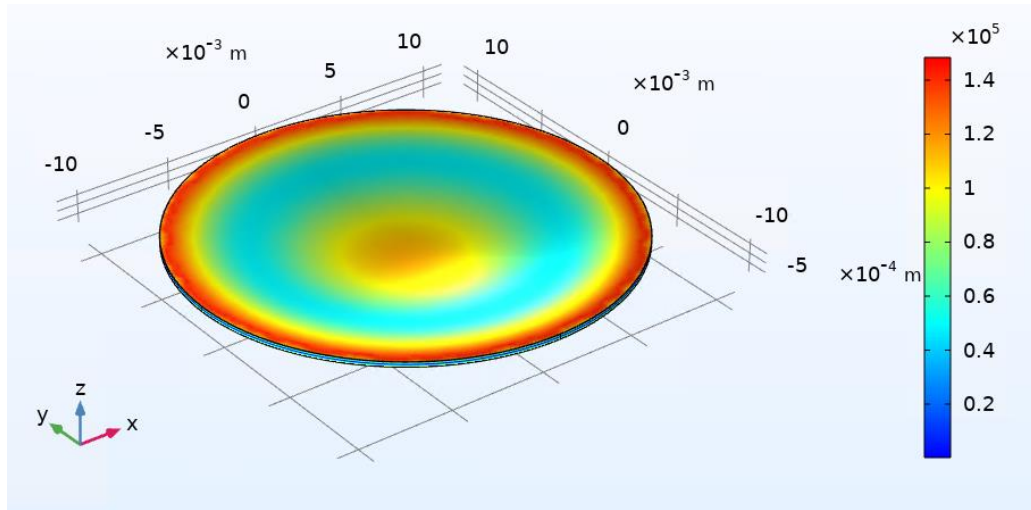
3.2. COMSOL numerical model

A numerical COMSOL model of a thin circular radially constrained plate under uniform load was constructed to calculate the von Mises Stress, which is a value used to determine if a given material will yield or fracture. The plate was at room temperature conditions, and pressure calculations assume the fluid is water. In COMSOL calculations, resulting von Mises stresses are

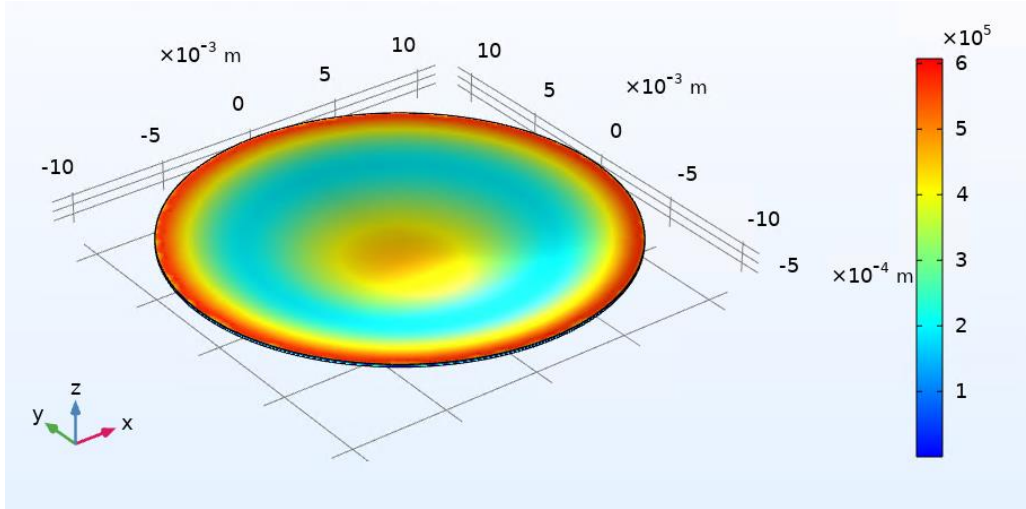
displayed with as pseudo-color map of the circular plate. For the three simulation cases displayed in Figure 10, the radius of stainless steel 316 plate is $a = 11.1\text{mm}$. For the case in Figure 10(a), $v = 1\text{ m/s}$ and $h = 10\text{mil}$, in Figure 10(b) $v = 0.5\text{ m/s}$, $h = 10\text{mil}$, and in Figure 10(c) $v = 0.5\text{ m/s}$, $h = 5\text{mil}$.



(a)



(b)



(c)

Figure 10 – COMSOL claculation of Von Mises stresses for (a) $v = 1$ m/s, $h = 10$ mil, (b) $v = 0.5$ m/s, $h = 10$ mil, (c) $v = 0.5$ m/s, $h = 5$ mil.

The maximum von Mises Stress are approximately 0.7 MPa, 0.14 MPa, and 0.6 MPa in Figures 14(a), 14(b), and 14(c). In comparison, σ_{\max} values calculated using Equation (1) for the same set of v and h values are 0.7 MPa, 0.18 MPa, 0.7 MPa, respectively. The values obtained from COMSOL simulations and the analytic model are in good agreement. These values of maximum stress are three orders of magnitude smaller than the YS or UTS of stainless steel 316. This suggests that the membrane is at a low risk of fracture.

4. Fabrication of Sensor Prototype

4.1. Fabrication of microwave cavity

Based on the results obtained from modeling and simulation of resonant transducer performance, preliminary design of the microwave cavity transducer was developed for fabrication in a machine shop. The side view of the cavity is shown in Figure 11. All dimensions are in units of inches. In this design, the cavity is assembled from a hollow cylinder, a thick cap at the bottom, and a thin diaphragm made from 10mil shim stock metal (1mil = 10^{-3} in). The thin diaphragm is held in place with a clamping ring. All the holes in the drawing are for 4-40 screws, which are the same size screws used for the K-band waveguide flange. In the design shown in Figure 2, microwave field is coupled into the cavity through a subwavelength aperture on the side of the cylinder. Compared to an earlier design with 0.116 in (3 mm), a smaller diameter aperture of 0.086 in (2.2mm) was chosen. For K-band mean frequency $f_{\text{mean}} = 22\text{GHz}$ and the corresponding free space wavelength $\lambda = 13.6$ mm, the diameter of the new aperture is 0.16λ . According to computer simulations, the Q factor of TE_{012} mode would be higher for the smaller aperture. The aperture is matched to the center of the waveguide. Coupling of the waveguide to the cylindrical cavity is accomplished by chamfering the side of a cylindrical cavity to obtain a flat surface. 3D rendering of the cylindrical cavity in Figure 2 shows the chamfered side surface and the small aperture for coupling microwave field into the cavity.

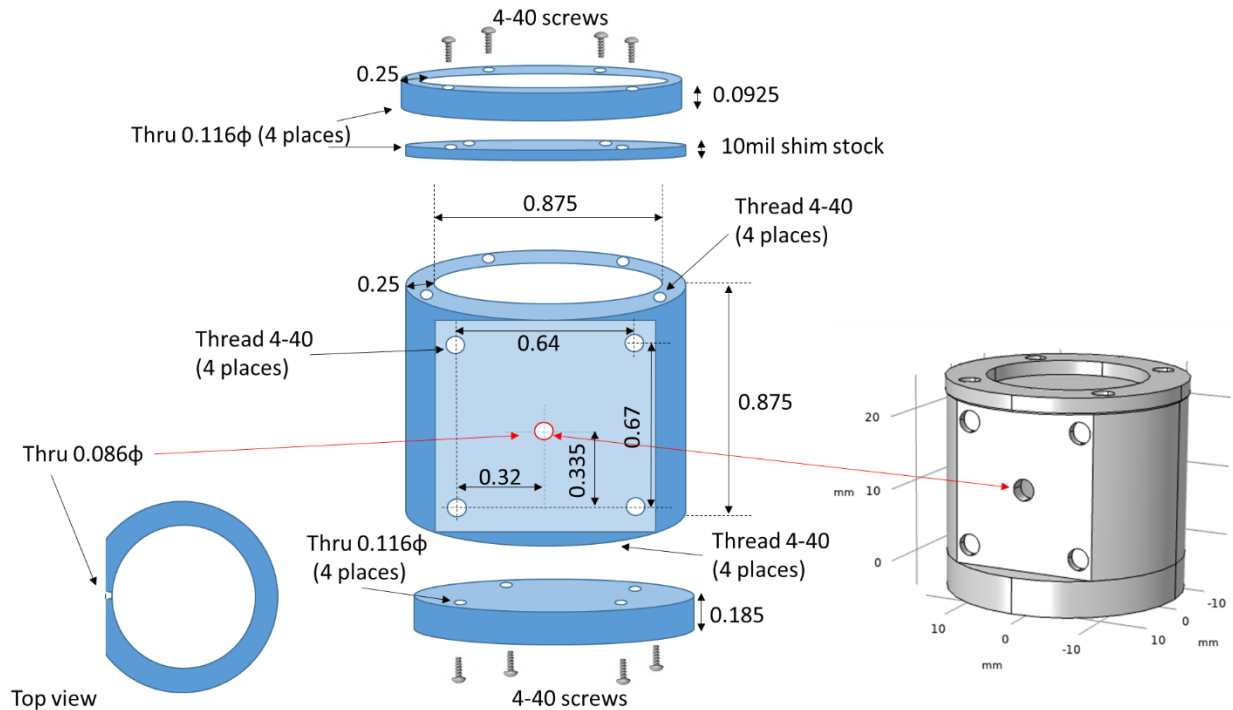


Figure 11 – Side view and 3D visualization of the cylindrical cavity design.

Visualization of WR-42 microwave K-band waveguide attached to cylindrical cavity is shown in Figure 12. The top view of the cylinder without the diaphragm is also shown in Figure 12. In

The image contains two technical drawings of a mechanical part. The left drawing is a 3D perspective view, and the right drawing is a 2D cross-sectional view.

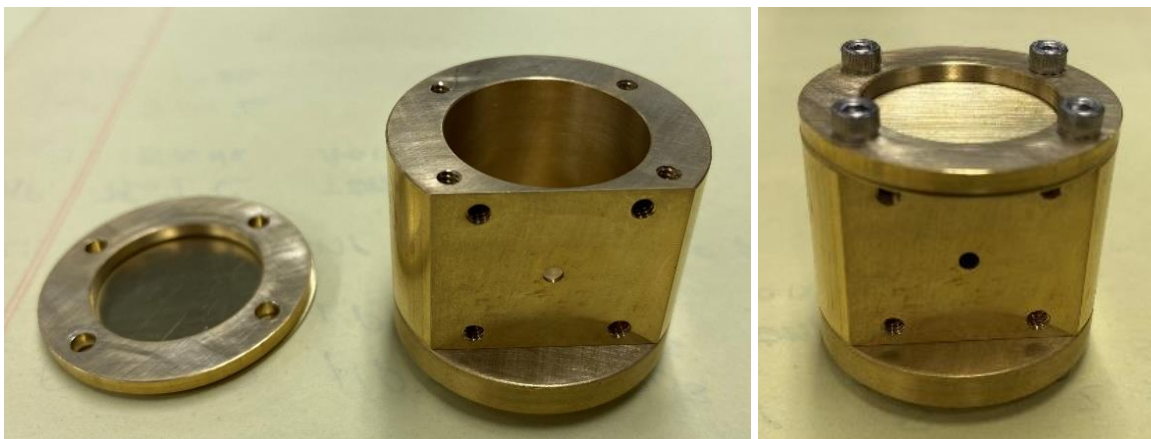
3D Perspective View (Left):

- The part consists of a cylindrical body with a flange on top and a rectangular block attached to its side.
- Dimensions are given in mm: 20, 10, 0, 40, 20, 0.

2D Cross-Sectional View (Right):

- The view shows the internal structure of the part, including a central hole and a rectangular block.
- Dimensions are given in mm: 5/32, 4-40, 0.633, 0.4375, 0.125, 0.25, 0.086, 0.02.
- Thread specifications are indicated: "Thread 4-40 (4 places)".

For proof-of-principle study, a cavity was fabricated from brass. Using brass instead of stainless steel saves cost on materials and machining. K-band brass cavity fabricated at Argonne Central Shop is shown in Figure 4. The left panel shows a photograph of the cavity with the top membrane removed. The panel on the right shows an assembled cylindrical cavity with stainless steel screws. With this design, the top membrane is interchangeable. The cavity in Figure 13 has a 10mil-thick membrane. In addition 9mil and 8mil-thick membranes have been fabricated for flow sensor performance testing.



19

The photograph in Figure 14 shows the microwave cavity coupled to a commercial WR-2 bulkhead waveguide. The waveguide is welded to a mounting plate for leak-proof insertion of microwave flow sensor into a pipe.



Figure 14 – Brass cavity coupled to WR-42 bulkhead waveguide

4.2. Fabrication of piping Tee adapter

A leak-proof assembly for insertion of microwave cavity into a flow stream was designed using a bulkhead WR-42 transducer and a PVC size 3 piping reducing Tee. The adaptor is thick disc with a concentric hole. The schematics and dimensions of the assembly cross-section are shown in drawing in Figure 15. The location of the adaptor is indicated with solid grey color. The adaptor rests against the notches in the pipe of the Tee near the intersection. The dimensions were chosen to position the cylindrical resonant cavity in the middle of size 3 pipe. The outer diameter of the adaptor matches the dimensions of the mounting plate of the WR-42 bulkhead waveguide. The inner diameter is large enough for insertion of cylindrical cavity into the piping Tee. The adaptor was machined from solid PVC cylinder in Argonne Central Shop.

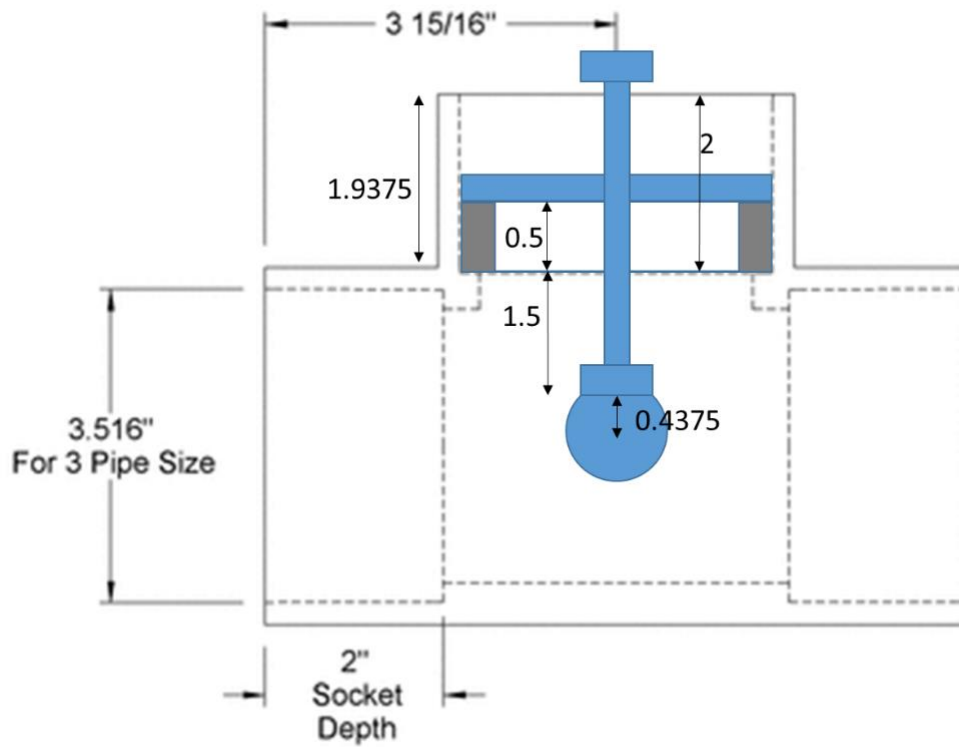


Figure 15 – Leak-proof assembly consisting of a piping Tee and WR-42 bulkhead waveguide for insertion of microwave cavity into fluid stream

Schematic drawing of the adaptor with all dimensions is shown in Figure 16. The adaptor is designed to fit inside size 3 pipe. The pattern of threaded blind holes in the adaptor is matched to that of the through holes on the mounting plate of the bulkhead waveguide.

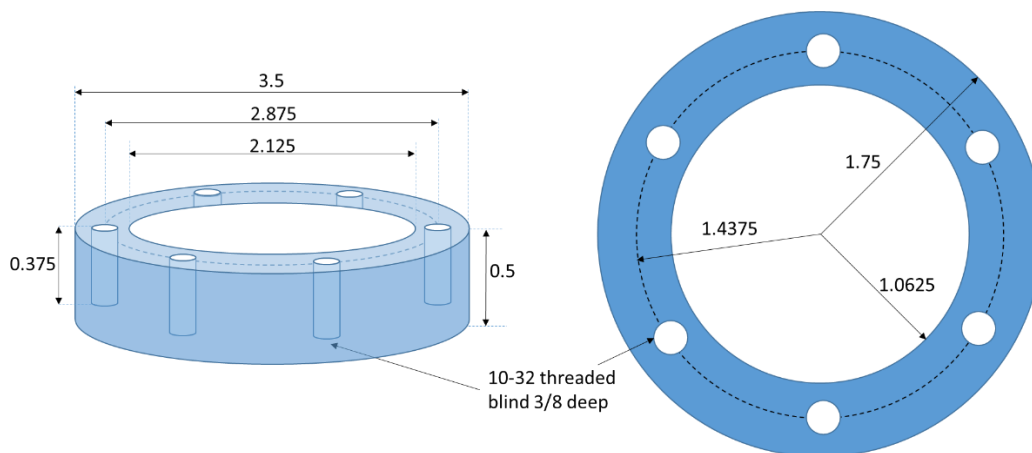


Figure 16 – Schematic drawing of adaptor for mounting WR-42 bulkhead waveguide in a piping Tee

Photograph of the PVC adaptor and WR-42 bulkhead waveguide installed in clear PVC piping Tee is shown in Figure 17. The adaptor is glued into the piping Tee. The photograph is taken before the mounting plate was attached with screws to the adaptor plate.



Figure 17 – Photograph of adaptor and WR-42 bulkhead waveguide installed in piping Tee

4.3. Electronic measurement system

Experimental setup consisting of the piping test article, microwave flow sensor, and microwave spectrum analyzer, is shown in Figure 18(a). In the setup, the cylindrical cavity is positioned in the middle of a PVC pipe with a bulkhead waveguide mounted on the side of the piping Tee. SMA (sub-miniature type A) cables are connecting the waveguide to VNA (vector network analyzer). Readout of the cavity spectrum is performed with a WR-42 waveguide microwave circulator, which isolates microwave reflection at the input to the cavity from microwave radiation of the cavity. Because microwave field is coupled into the cavity through a subwavelength hole, most of microwave power is reflected at the entrance to the cavity. If not suppressed, the reflected signal will overlap with radiation from the cavity, thus contributing a strong background to the signal measured with VNA.

Microwave circulator connected to the waveguide is shown in better details in zoomed-in image in Figure 18(b). SMA cable from VNA Port 1 is connected to the input (port 1) of the circulator. Port 2 of the circulator is connected to the waveguide. Port 3 of the circulator is to VNA port 2 with a cable marked with red tape. The signal measured with VNA is S_{21} . Isolation between circulator ports is approximately 20dB. Therefore, there is leakage of back-reflected signal which contributes to S_{21} background.



(a)



(b)

Figure 18 – (a) Electronics and mechanics of the experimental setup for proof-of-principle testing (b) Waveguide microwave circulator is used for excitation and readout of microwave cavity

5. Preliminary Proof-of-Principle Tests

5.1. Setup for proof-of-principle dry test

An experimental setup was assembled for proof-of-principle transducer dry testing with calibrated weights. The objective of this test was to obtain preliminary estimates of transducer measurement sensitivity. Microwave measurements were performed with a portable PXIe chassis vector network analyzer (VNA) with 300 kHz to 26.5 GHz frequency range. Figure 19 shows a photograph of the laboratory setup for the dry test. The PXIe has a graphical user interface (GUI) with a range of built-in libraries for signal processing and data visualization. Note that the portable PXIe VNA will be part of the setup for the next stage of the project involving fluid flow sensing.



Figure 19 – Experimental setup for transducer dry testing with a set of calibrated weights

A zoomed-in image of a 50 g calibrated weight placed on the resonant cavity's thin membrane is shown in Figure 20. Note that in water test, as the membrane deflects due to pressure, water will conform to the membrane shape and continue to exert pressure on the caved section. On the contrary, a body with a rigid surface, such as the weight in Figure 20, will loose contact with the caved-in section of the membrane. To partially compensate for this effect a piece of foam was glued to the bottom of each weight. However, it should be noted that transducer response in a dry test with a rigid body is most likely weaker than the response due to pressure from the same weight of water column.

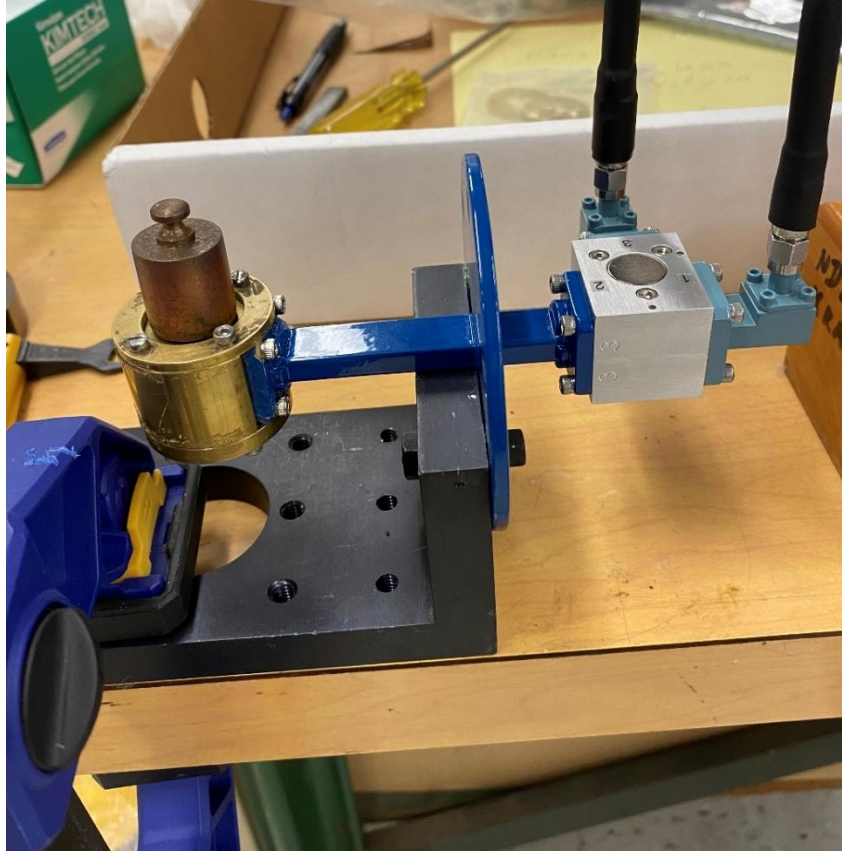


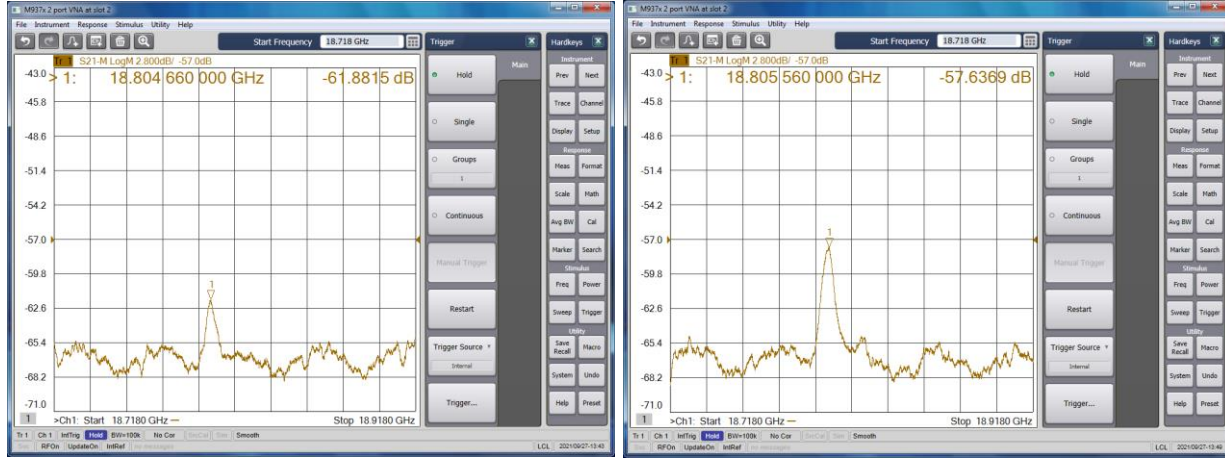
Figure 20 – Dry test measurement of transducer response to pressure from a 50g weight

5.2. Proof-of-principle dry test measurements

Preliminary measurements of transducer response in a dry test with calibrated weights were conducted using a PXIe microwave VNA. In the sweep across K-band spectrum (18 GHz – 26.5 GHz), four microwave cavity resonant frequencies were identified at which measurable response was recorded: 18.8 GHz, 21.3 GHz, 22.5 GHz, 23.7 GHz, and 25.8 GHz. The strongest signals were observed at 18.8 GHz and 22.5 GHz resonant frequencies. The sizes of the simulated cylindrical resonator model in Section 2 ($2R = 0.7$ in), and actual experimental resonator described in Section 4 ($2R = 0.875$ in), differ by a multiplicative factor of 1.25. Resonant frequencies of the TE_{011} and TE_{012} modes of the simulated cylindrical resonator ($2R = 0.7$ in) are 22.2 GHz and 26.5 GHz. With linear scaling, TE_{011} and TE_{012} modes of the experimental resonator ($2R = 0.875$ in) are expected to be at 17.8 GHz and 21.2 GHz, respectively. Both of these numbers are off by 1 GHz from the observed responses. This will be further investigated with COMSOL modeling of the resonator with dimensions equal to that of the experimental one.

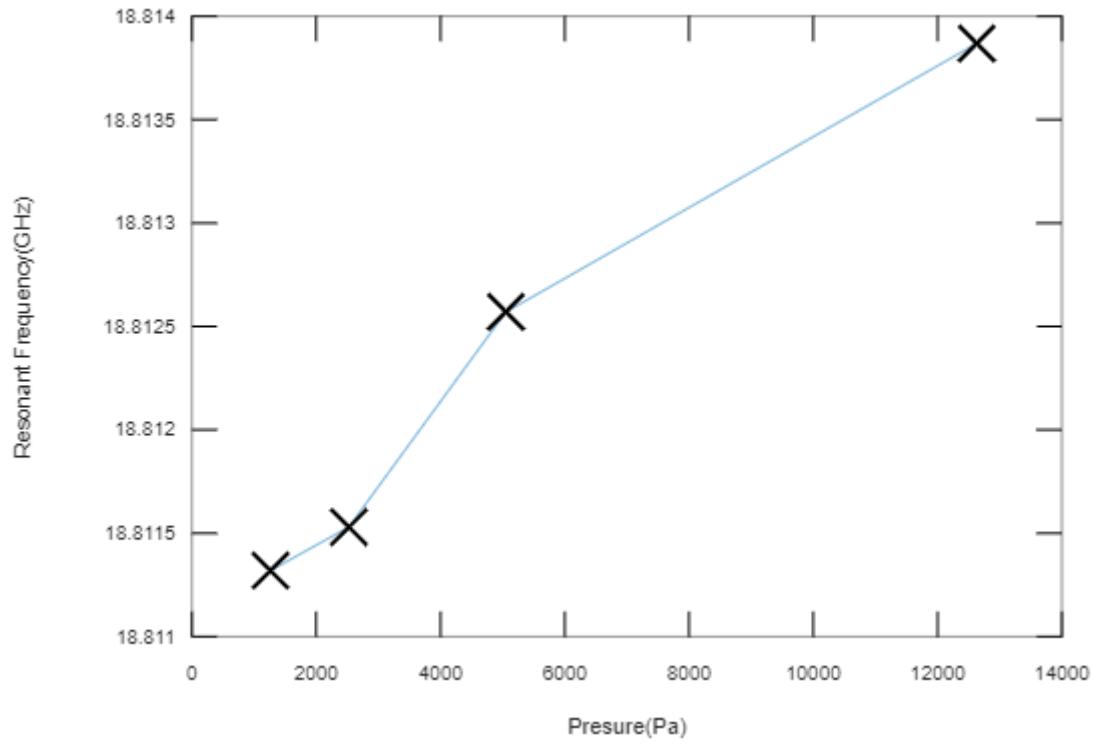
Examples of GUI interface for signal measurement due to applied pressure from different calibrated weights are shown in Figure 21. Both signals were recorded for transducer response near the 18.8 GHz resonant frequency. Figures 21(a) and 21(b) show the responses due to pressure from 50 g and 100 g masses, respectively. Signal processing consists of background subtraction, averaging and signal smoothing. Background subtraction involves recording the spectral response

of the resonator before pressure is applied, and subtracting background signal from the spectrum measured after pressure is applied. When the load is removed, the signal disappears. Measurements were shown to be stable and repeatable.

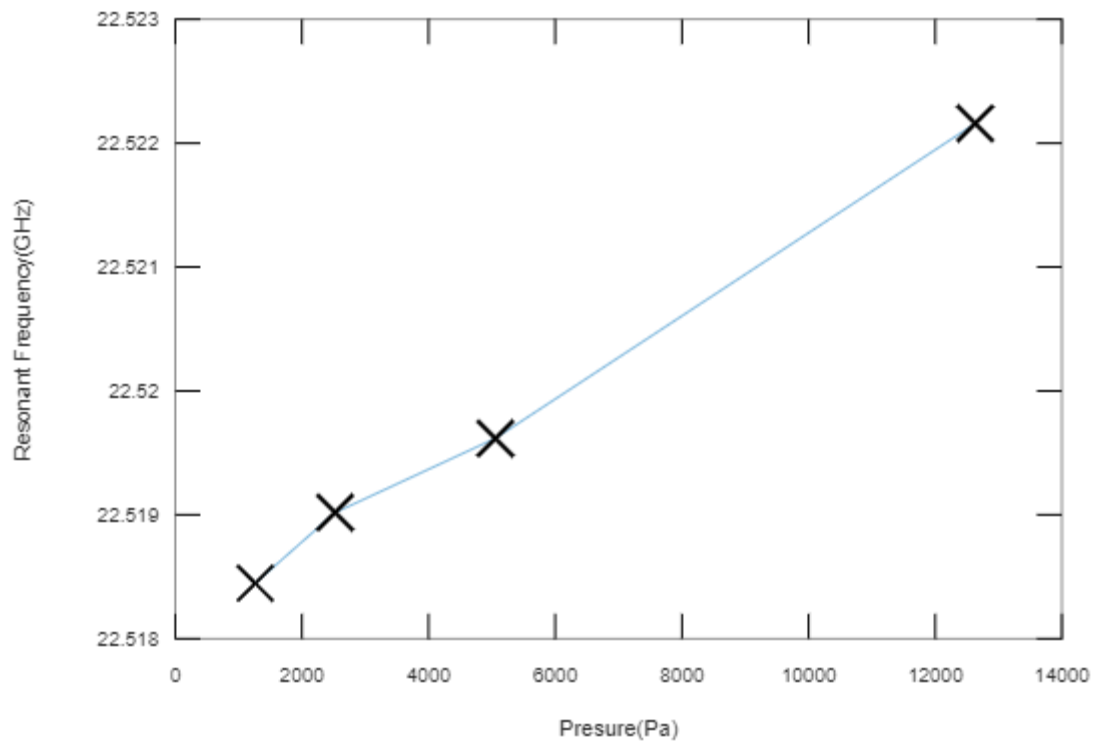


(a) (b)
Figure 21 – GUI visualizing transducer response near 18.8GHz resonant frequency due to pressure applied calibrated weights: (a) 50g, (b) 100g.

Four masses of 50 g, 100 g, 200 g, 500 g were used to measure transducer responses near 18.8 GHz and 22.5 GHz resonant frequencies, which are displayed in Figures 22(a) and 22(b), respectively. The graphs show resonant frequency as a function of pressure. The latter is calculated by dividing the weight of the mass by the area of the transducer membrane. Both graphs show a nearly linear monotonic increase of transducer resonant frequency with increasing pressure, which is consistent with findings of analytical and computational studies in Section 2. From Figure 22, doubling of the pressure results in approximately 1 MHz spectral shift of the resonant frequency. As discussed above, the pressure due to fluid and the pressure due to a rigid solid weight might not be equivalent. However, as a rough guide, the smallest pressure measurement of 1260 Pa (due to 50 g mass) is equivalent to pressure produced by water flowing at 1.6 m/s velocity. The fact that reasonably good response is observed at two spectrally close frequencies can be used for coincident detection to increase confidence in detection of weak signals.



(a)



(b)

Figure 22 – Transducer resonant frequency vs. applied pressure from 50 g, 100 g, 200 g, and 500 g weights. Responses are near cavity resonant frequencies (a) 18.8 GHz, (b) 22.5 GHz

6. Conclusions

We describe the development of a K-band microwave cylindrical cavity for preliminary proof-of-principle tests. This sensor is a hollow metallic cylindrical cavity, which can be fabricated from stainless steel, and as such is expected to be resilient to radiation, high temperature and corrosive environments of MSCR and SFR. The principle of sensing consists of making one wall of the cylindrical cavity flexible enough so that dynamic pressure, which is proportional to fluid velocity, will cause membrane deflection. Membrane deflection causes change in the cavity volume, which leads to a shift in the resonant frequency of the cavity.

Feasibility of the flow sensor was initially investigated using analytical derivations and COMSOL computer simulations. A right cylinder geometry stainless steel cavity with diameter of 0.7 in was investigated. We chose a membrane thickness of 10 mil, so that an anticipated corrosion rate of 1 mil/year would affect no more than 10% of the membrane. Results of computer simulations indicate a measurable sensitivity to flow for this transducer design. Computer simulations indicated that the best sensitivity to flow-induced membrane displacement will be achieved when the cavity is excited in TE_{011} or TE_{012} modes. We also performed analytical and computational investigation of the mechanical integrity of the sensor membrane. The mechanical model of the transducer membrane is a thin radially clamped circular plate subjected to a uniform load. Stresses on the membrane are calculated with an analytic model, and with numerical COMSOL model. Maximum stresses on the plate are compared to yield strength (YS) and ultimate tensile strength (UTS) to determine if the plate could undergo plastic deformation or failure. Calculated maximum stresses are three orders of magnitude smaller than the YS and UTS. This indicates that the sensor should operate in the linear elastic deflection regime, and the likelihood of failure is relatively small.

A cylindrical cavity with a side feed was designed for operation in K-band (18 GHz – 26.5 GHz), and fabricated from brass. The dimensions of the cavity were selected to match the flange of a WR-42 (K-band) waveguide. Once fabricated, the cavity was connected to a WR-42 bulkhead waveguide. A microwave circulator was installed in the setup to suppress the effect of reflections at the cavity entrance by increasing the isolation between the input and the output port. A test article with a leak-proof insert connecting the microwave sensor to a piping Tee was developed as well. Preliminary spectral characterization of the cavity response was performed using a PXIe portable microwave VNA. The PXIeGUI comes with built-in routines for visualization of the measurement signal, which includes automated background subtraction, averaging and smoothing. Proof-of-principle dry test was performed with a set of calibrated weights. Applying mechanical pressure to cavity membrane showed a measurable shift in the microwave resonant frequency. Resonant frequency increases monotonically and it is nearly linear, which is qualitatively consistent with the results of analytical and numerical modeling.

The next steps for this project will involve measurement of spectral shift in water flow tests. The piping Tee will be inserted into a water flow loop, where the flow sensor will be used to measure fluid velocity. In parallel, signal processing algorithms will be developed to improve detection and visualization of displayed signals and to automate the measurement process.

References

1. E. Blandford, K. Brumback, L. Fick, C. Gerardi, B. Haugh, E. Hillstrom, K. Johnson, P.F. Peterson, F. Rubio, F.S. Sarikurt, S. Sen, H. Zhao, N. Zweibaum, “Kairos Power Thermal Hydraulics Research and Development,” Nuclear Engineering and Design 364, 110636 (2020).
2. K. Aoto, P. Dufour, Y. Hongyi, J. P. Glatz, Y. Kim, Y. Ashurko, R. Hill, N. Uto, “A Summary of Sodium-Cooled Fast Reactor Development,” Progress in Nuclear Energy 77, 247-265 (2014).
3. K. Korsah, R.A. Kisner, C.L. Britton Jr., P. Ramuhalli, D.W. Woodan, N.C. Anheier, A.A. Diaz, E.H. Hirt, R.B. Vilim, H.T. Chien, S. Bakhtiari, S.H. Sheen, N. Gopalsami, A. Heifetz, S.K. Tam, Y. Park, B. Upadhyaya, A. Stanford, “Assessment of Sensor Technologies for Advanced Reactors,” PNNL-SA-132062 (2017).
4. A. Heifetz, D. Lisowski, M. Weathered, Y. Momozaki, H.T. Chien, S. Bakhtiari, “Preliminary Review Analysis of Distributed Sensors for Versatile Test Reactor (VTR) Environment,” Argonne National Laboratory ANL/NSE-18/11 (2018).
5. D. Holcomb, R. Kisner, S. Cetiner, “Instrumentation Framework for Molten Salt Reactors,” ORNL/TM-2018/868 (2018).
6. A. Heifetz, V. Ankel, D. Shribak, S. Bakhtiari, A. Cilliers, “Microwave Resonant Cavity-Based Flow Sensor for Advanced Reactor High Temperature Fluids,” Proceedings of 12th Nuclear Plant Instrumentation, Control and Human-Machine Interface Technologies (NPIC-HMIT 2021), 526-533 (2021).
7. A. Heifetz, D. Shribak, S. Bakhtiari, E.R. Koehl, “Design of Microwave Resonant Cavity Transducer,” Argonne National Laboratory ANL-21/15 (2021).
8. S. Timoshenko and S. Woinowsky-Krieger, *Theory of Plates and Shells*, 2nd Edition, McGraw- Hill, New York, (1964).
9. G.L. Hoffman, M.C. Billone, J.F. Koenig, J.M. Kramer, J.D.B. Lambert, L. Leibowitz, Y. Orechwa, D.R. Pedersen, D.L. Porter, H. Tsai, and A.E. Wright, “Metallic Fuels Handbook,” ANL-NSE-3 (2019).
10. J.K. Fink and L. Leibowitz, “Thermodynamic and Transport Properties of Sodium Liquid and Vapor,” ANL/RE-95/2 (1995).
11. M.S. Sohal, M.A. Ebner, P. Sabharwall, P. Sharpe, “Engineering Database of Liquid Salt Thermophysical and Thermochemical Properties,” INL/EXT-10-18297 (2010).
12. S. Bakhtiari, T. Gonnot, T. Elmer, H.T. Chien, D. Engel, E. Koehl, A. Heifetz, “Evaluation of Microwave Cavity Gas Sensor for In-Vessel Monitoring of Dry Cask Storage Systems,” *Proceeding of AIP Conference* 1949, 110004 (2018).
13. S.L. Schrock, J.N. Baysden, R.L. Miller, D.E. Lohr, “Sodium Corrosion of Westinghouse Liquid Metal Fast Breeder Reactor (LMFBR) materials” In: Draley J.E., Weeks J.R. (eds) *Corrosion by Liquid Metals*. Springer, Boston, MA (1970).

14. G. Zheng, B. Kelleher, G. Cao, M. Anderson, T. Allen, K. Sridharan, “Corrosion of 316 stainless steel in high temperature Li_2BeF_4 (FLiBe) salt,” *Journal of Nuclear Materials* 461, 143-150 (2015).
15. E. Sooby-Woods, M. Alamaniotis, A. Heifetz, “Gaussian Process Ensemble for Corrosion Modeling and Prediction in Molten Salt Reactors,” *Proceedings of 12th Nuclear Plant Instrumentation, Control and Human-Machine Interface Technologies (NPIC-HMIT 2021)*, 239 – 250 (2021).
16. D. Kultgen, C. Grandy, E. Kent, M. Weathered, D. Andujar, and A. Reavis, “Mechanisms Engineering Test Loop – Phase I Status Report – FY2018,” ANL-ART-148, ANL-METL-14 (2018).
17. A. Heifetz, S. Bakhtiari, E.R. Koehl, D. Aronson, “Fabrication and Preliminary Demonstration of Microwave Resonant Cavity Transducer Performance,” *Argonne National Laboratory ANL-21/38* (2021).



Nuclear Science and Engineering (NSE) Division

Argonne National Laboratory

9700 South Cass Avenue, Bldg. 208

Argonne, IL 60439

www.anl.gov



Argonne National Laboratory is a U.S. Department of Energy
laboratory managed by UChicago Argonne, LLC